

Computer-controlled microresonator soliton comb system automating soliton generation and expanding excursion bandwidth

LEFENG ZHOU, YANG SHEN, CHAOXIANG XI, XIN HUANG,  AND GUANGQIANG HE* 

State Key Laboratory of Advanced Optical Communication Systems and Networks, Department of Electrical Engineering, Shanghai Jiao Tong University, Shanghai 200240, China
*gqhe@sjtu.edu.cn

Abstract: A computer-controlled dual-laser dissipative Kerr soliton (DKS) comb system is established. The system can automatically and robustly access the single soliton state by controlling two lasers and a power meter. It can adapt to different working environments. Even if the resonant frequency drifts by a few GHz, or the pump power drifts by 20%, the system still stably accesses the single soliton state. Moreover, the system architecture allows users to operate the system easily and flexibly. By tuning the pump and auxiliary lasers synchronously, the range of the comb frequency scan (excursion bandwidth) is expanded from 700 MHz to over 10 GHz.

© 2022 Optica Publishing Group under the terms of the [Optica Open Access Publishing Agreement](#)

1. Introduction

The optical frequency comb [1,2], which consists of equidistant spectral lines, is a powerful tool for connecting radio and optical frequency. The dissipative Kerr soliton (DKS) based on microresonators [3,4], whose spectrum appears as an optical frequency comb, receives extensive attention due to its compactness, high repetition rates from GHz to THz, and low noise characteristics. The potential of DKS combs has been greatly developed in many fields, such as optical communications [5], ranging [6,7], frequency-modulated continuous-wave (FMCW) LiDAR [8], low phase noise microwave generation [9], optical frequency synthesis [10], dual-comb spectroscopy [11,12], and quantum key distribution [13]. Microresonators of different materials [14–18] are studied to generate single solitons. The silicon nitride (Si_3N_4) is favored because its manufacturing platform is compatible with CMOS, which is conducive to its integrated and large-scale production and application.

The single soliton state must be robustly accessed to promote the application of DKS combs. However, it is not an easy task because of the thermal instability preceding the stable soliton state. Many methods to access a single soliton state are proposed, such as fast sweeping of the pump laser [3], power kicking [19], backward tuning [20], pulse-driven scheme [21], generating Brillouin laser in the cavity [22], and thermal control with intensity modulator [23], with heater [24], and with auxiliary laser [25]. Some other methods rely on the dispersion engineering, such as designing nearly degenerated mode families [26], or utilize the material properties, like the photorefractive effect of lithium niobate [14]. Among them the dual-laser scheme (with an auxiliary laser) is particularly attractive, because it not only eases soliton generation, but also provides two extra degrees of freedom to control the system, i.e., the power and frequency of the auxiliary laser [27]. They can be utilized to stabilize the comb [28], to generate reconfigurable soliton crystals [29], to make the solitons self-start and bidirectionally switch by thermal overcompensation [30], and to extend the spectrum [31], etc.

Though there are lots of researches of DKS combs in the laboratory, it still takes a long time to improve them for industrial applications. The system for generating DKS combs needs simpler operation and lower costs. So, a program-controlled single soliton microcomb source is

developed [32]. In some cases, expensive devices are avoided in the system to cut costs, such as using DP-MZI [33], or DFB lasers only [34]. In this paper, we demonstrate a computer-controlled dual-laser DKS comb system with improved control logic, compared with the previous works. Our system can robustly access the single soliton state by controlling a pump laser, an auxiliary laser, and a power meter. There are no other costly devices such as high-speed detectors in the system. Based on a personal computer, the system allows users to operate the equipment quickly and orderly by programming. Since the software implementation is very flexible, power monitoring, signal processing, and feedback can be seamlessly cascaded. We propose a criterion of power drop ratio to infer the soliton number in the cavity. This criterion exhibits much better anti-interference ability than setting power threshold only [32]. Besides, our automated procedure is compatible with other feedback stabilization after the soliton is generated. Our system is a prototype for industrial applications.

Comb lines need to be modulated in many applications, such as spectroscopy [35] and FMCW LiDAR [8]. The range that one comb line can scan, i.e., the excursion bandwidth, is inversely proportional to the distance resolution of FMCW LiDAR. Many methods are invented to increase the excursion bandwidth, such as applying feedforward signals on both the laser and heater [36]. In this paper, we expand the excursion bandwidth greatly. First, we measure the soliton step length, which is 700 MHz. Then, we synchronize two lasers to expand the excursion bandwidth to over 10 GHz. Synchronous operation is very easy to realize through our computer-controlled system. It is expected to improve the distance resolution of FMCW LiDAR by an order of magnitude.

2. Experiment setup

2.1. Design of the microresonator

The soliton is generated in a microresonator on the Si_3N_4 chip. The structure of the microresonator is shown in Fig. 1(a). The radius of the ring waveguide is 240 μm . The geometry of the waveguide cross-section is shown in Fig. 1(b). We numerically simulate the dispersion of TE mode to assure anomalous dispersion. We also simulate how the gap between the ring and straight waveguide affects the external loss, because it is better to achieve critical coupling, where the external loss is equal to the internal loss. To reduce the influence of manufacturing instability on internal loss, microresonators with a series of gaps are fabricated. In our experiments, we use the one with a 0.45 μm gap.

2.2. Characterization of the microresonator

We characterize the dispersion, FSR, and Q of the microresonator. We sweep across a wide range around 1550 nm to obtain the transmission spectrum, part of which is shown in Fig. 1(d). The integrated dispersion D_{int} and FSR can be extracted from the spacing of resonances, as shown in Fig. 1(c). The transmission reveals that $\text{FSR} = 95.1$ GHz and $D_2/2\pi = 9.8 \times 10^5$ Hz. Then we slowly sweep over the resonance at 1551.4 nm and fit the transmission with Lorentzian curve to calculate Q of this resonance, which is shown in Fig. 1(e). We estimate that the intrinsic quality factor Q_{in} is 4.1×10^6 and the external quality factor Q_{ex} is 7.2×10^6 . The width of the resonance is 74.1 MHz, corresponding to the overall $Q = 2.6 \times 10^6$.

2.3. Experiment setup of soliton generation

The experiment setup is shown in Fig. 2(a). The pump laser (PPCL550) and the auxiliary laser (PPCL300) can be continuously tuned by up to ± 30 GHz around a wavelength preset near 1550 nm. Though the internal control loop makes the output frequency jitter by tens of MHz, it exerts little influence on the soliton generation in our experiment scheme. The EDFAs can amplify the laser power to 33 dBm at most. Two FPCs control the polarization modes, each of which

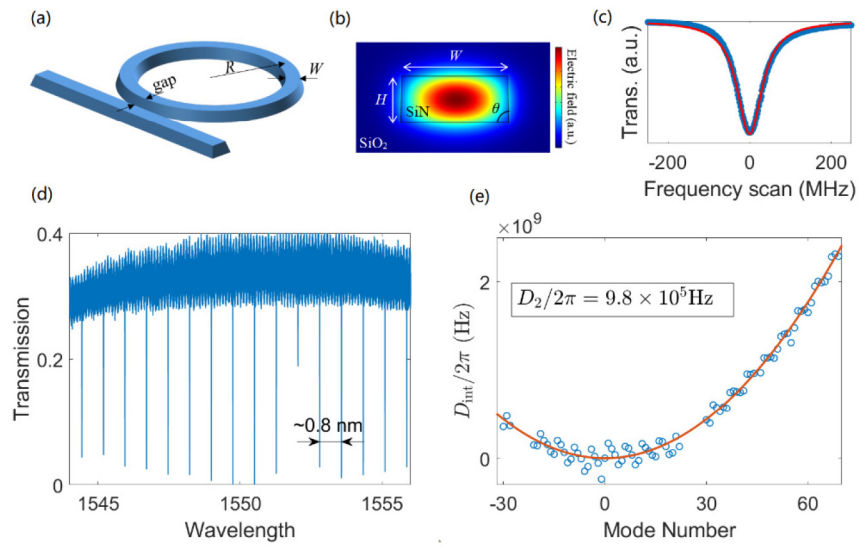


Fig. 1. (a) Schematic of microresonator. $R = 240 \mu\text{m}$, $W = 1.8 \mu\text{m}$, and $\text{gap} = 0.45 \mu\text{m}$. (b) The cross-section of the waveguide in simulation with TE mode pump. $H = 0.8 \mu\text{m}$, and $\theta = 89^\circ$. (c) One specific resonance at 1551.4 nm . The resonance is fitted with a Lorentzian curve (red) to calculate its quality factor (Q). We estimate that the intrinsic $Q = 4.1 \times 10^6$. (d) Transmission spectrum of the resonator. The resonances are equidistant at $\sim 0.8 \text{ nm}$. (e) The integrated dispersion D_{int} .

corresponds to its unique dispersion in the waveguide. The polarization control is necessary, because the resonances corresponding to two different modes are seldom at the same frequency so that the pump light which consists of two modes is unable to inject all the power into the cavity. Moreover, via FPCs, we make the pump and auxiliary light propagate in orthogonal modes to reduce the influence of the auxiliary light on soliton generation. Then two beams of laser light are coupled into the waveguide through fiber lenses in opposite directions, with two circulators that separate the input and output light. The output of the auxiliary laser is directly monitored by a power meter (sampling rate 1 kSa/s at most). The output of the pump laser is divided into two paths by a BS. One path is monitored by the power meter, while the light on another path passes through two FBGs that reject both the pump light and the reflected auxiliary light, i.e., only the light generated by nonlinear effects remains. This remaining portion of the light is again split by a BS, with one path monitored by the power meter and another path left for other usages as the soliton output port. In our experiments, the output port is connected to an OSA which is irrelevant to system control, so it is convenient for the experimenters to observe the system state.

We develop a computer-controlled system based on our schematic shown in Fig. 2(a). All electrical devices, including the two lasers and the power meters, are controlled by a computer. We abstract the system into a three-layer model shown in Fig. 2(b), with (1) optical layer, (2) communication layer, and (3) applications. The first layer is fully optical. The lasers generate light physically; and the light field evolves in the cavity and finally generates solitons. In other words, the optical layer is where the physical process takes place. The second layer is the abstraction of the first layer. A laser is only an object whose main properties are wavelength and output power. The intracavity situation is characterized by reading of the power meter. That is to say, users at the second level do not worry about the physical operation of the devices. With one line of command, users can tune the laser to the frequency that they demand, or read the output power of the system, etc. In detail, we use serial ports complying with the RS-232 standard to

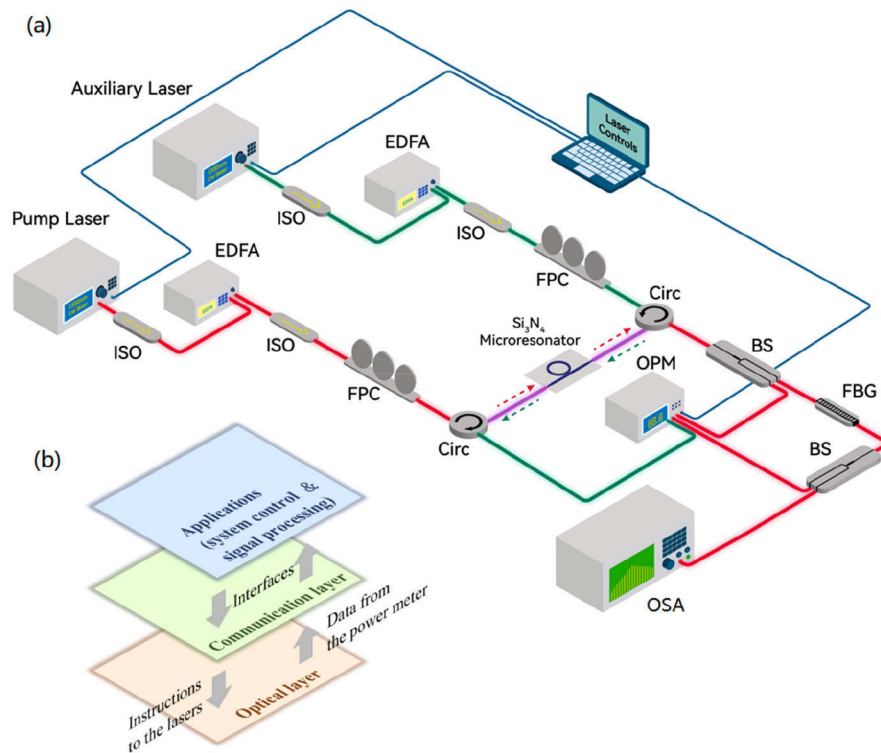


Fig. 2. (a) System schematic. The blue lines are electrical cables. The other colored lines are single-mode fibers. The pump and auxiliary laser fibers are distinguished by colors. ISO: isolator. EDFA: Erbium-doped fiber amplifier. FPC: fiber polarization controller. Circ: circulator. BS: beam splitter. OPM: optical power meter. FBG: fiber Bragg grating. OSA: optical spectrum analyzer. (b) Three-layer model, a universal architecture of the electrical control system.

connect all the electrical devices. We implement the codecs which convert information between bit streams in the RS-232 format and signals intelligible to human. As a result, the second layer provides users with interfaces that control the lasers and power meter. Based on these interfaces, we develop some applications that cascade a certain series of commands. These applications allow us to make complex operations in a fast and ordered way. An automation script that stably accesses the single soliton state is developed, as one example of the applications. All programs are written in MATLAB for rapid development and verification. However, since the architecture that we propose is universal, it can be implemented on any platforms, e.g., on MCU for better integration.

3. Results

3.1. Automating soliton generation

Our system can easily automate soliton generation, as we show in [Code 1](#) (Ref. [37]). An automation script imitates and replaces manual operation. The control flow is as follows.

Firstly, the two lasers are enabled. The pump laser outputs at ~ 1552.3 nm and the auxiliary laser at ~ 1557.1 nm. The pump laser and auxiliary laser are amplified to 30.5 dBm and 32.5 dBm respectively. After several optical devices and one facet of the waveguide (1.3 dB/facet loss), the on-chip pump power is ~ 26 dBm, and the auxiliary laser power is ~ 27.5 dBm. We

make the pump light and the auxiliary light propagate in two orthogonal modes. This can be done using the FPCs and the power meter. We adjust the FPCs to maximize the transmitted pump power, and to minimize the transmitted auxiliary laser power. Then the pump mode will belong to the same mode family that we describe in section 2.2. The soliton can also be generated if the same mode is used, i.e., both transmitted powers are maximized, but without a perfect spectral sech^2 envelope. Here in our system, the FPCs are not electrically controllable. But if they can be driven electrically, polarization control can be easily automated, since we only need to use the optimization algorithm to make the power reading reach the extremums.

Secondly, while the pump laser remains stationary, the auxiliary laser is tuned by 30 GHz from blue to red with a speed of 4 GHz/s to find a resonance. At the same time the power meter records the transmission, which is shown in Fig. 3(a). These transmissions are the typical saw-tooth waveforms. Differentiating the waveforms will highlight the sudden power change where the laser reaches the red detuning, which is shown in Fig. 3(b). Though the frequency of the resonance drifts by a few GHz, it can be stably located by wide-range sweep without any parameter change in the program.

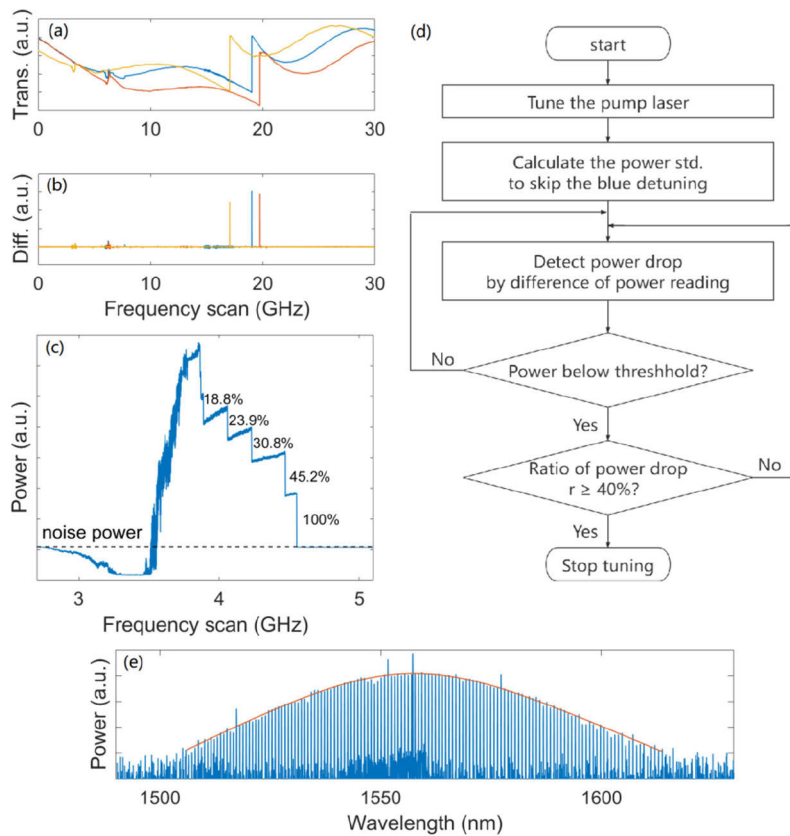


Fig. 3. (a) The transmission of the auxiliary laser in three experiments, in 10 mW/div. (b) Differentiation of the auxiliary laser transmission. (c) The output power of the system, in 10 mW/div. The ratios of power drop are marked beside the corresponding steps. (d) The flowchart of the algorithm. (e) The spectrum of the single soliton state in 5 dB/div. The envelope of the spectrum is fitted by the sech^2 curve.

Thirdly, we tune the auxiliary laser again but stop it at 9.5 GHz before the red detuning. How close it is to the resonance should still be determined by experiments, though our system tolerates

the frequency deviation of several GHz. A frequency too far from the resonance will weaken the heat compensation of the auxiliary laser, while a frequency too close to the resonance will excite strong nonlinear effects in the cavity, impairing the soliton generation.

Fourthly, the pump laser is tuned from blue to red to access the soliton state. The transmission of the pump laser is recorded by the power meter after two FBGs rejecting the pump and reflected auxiliary power. Hence the reading represents the sum of background noise power P_{noise} and the power caused by nonlinear effects, e.g., the power of solitons. We suppose that P_{noise} is a constant, so that it is measured at the beginning of pump tuning. Then, we calculate in real time the standard deviation of power reading to skip the blue detuning area where the intracavity power fluctuates dramatically. After reaching the red detuning area, our automation script can discern the intracavity situation and stop tuning when the single soliton state is accessed. The key algorithm is as follows, and shown in Fig. 3(d).

We differentiate the power reading to detect soliton number switching. Once the switching is detected, the script should identify the number of solitons existing in the cavity. This identification is achieved by two criteria. The first criterion is the absolute power reading. The power of a single soliton is limited so that the first criterion can reduce the solitons to a small number. The second criterion, which enhances the anti-interference of our system, is the ratio of power drop. Let P_{before} denote the power reading before soliton number switching, and P_{after} denote the power reading after soliton number switching. We define the ratio of power drop as $r = (P_{\text{before}} - P_{\text{after}}) / (P_{\text{before}} - P_{\text{noise}})$. Under the assumption that all solitons contribute the same power, soliton switching from N to $N-1$ will make the soliton power drop by $1/N$. Hence the ratio r indicates how many solitons there are in the cavity. Following these two criteria, we can access the single soliton state robustly.

The intervals in these criteria should be determined via experiments. As shown in Fig. 3(c) that $r_{N \rightarrow N-1} < 1/N$, the power drop caused by soliton switching influences the intracavity thermal equilibrium, increasing the frequency of the resonance, thus increasing the pump detuning and the power of each soliton. The difference between $r_{N \rightarrow N-1}$ and $1/N$ depends on the degree to which the auxiliary pump dominates the thermal effects in the cavity. Therefore, the optimal intervals in these criteria should be found in the experiments. In our automation script, a necessary condition that the single soliton state is accessed is that $r \geq 40\%$.

We should note that the first criterion is also crucial to the robustness of the system. The criterion of absolute power threshold guarantees a small number of solitons (≤ 3) before switching, which makes the second criterion more effective. This is because distinguishing $1/N$ with smaller N is easier, and also because annihilation of two or more solitons is difficult to identify when $N \geq 4$.

The final spectrum is shown in Fig. 3(e). The spectral envelope exhibits a typical sech^2 shape, which is shown in Fig. 3(e) red curve. Our system works properly under the circumstance that the single soliton can be manually generated, but faster than manual operation. Then we deliberately interfere with pump power to test the robustness of the system. In our experiments, $\pm 20\%$ pump power change does not affect program operation. High fault-tolerance provides the anti-interference ability, and also facilitates program debugging.

It is possible to automate the system further. The existence of the soliton is monitored, and the script can be automatically rerun after the soliton vanishes. What is more, the auxiliary laser provides two extra degrees of freedom, frequency and power, which can be used to stabilize the comb. Our script that automates soliton generation is compatible with other stabilization procedure [28].

3.2. Expanding excursion bandwidth

In our dual-pump system, the comb line can be continuously tuned back and forth in a large range with the aid of thermal effects. In many applications such as the parallel FMCW LiDAR, it

is necessary to continuously change the frequency of each comb line. The larger the excursion bandwidth, the higher the resolution. When the frequency of the pump light is moved, all the comb lines will move with it, leaving the repetition rate nearly unchanged. Though Raman nonlinearity will couple the repetition rate to the pump detuning, we estimate in theory that there is ~ 1 MHz repetition rate change at most in our case [38,39], thus neglecting its influence. In order to maintain the single soliton state, the detuning $\delta = \omega_0 - \omega_p$ is limited, which means that the excursion is restricted by the length of “soliton step”. To expand the excursion under the condition of limited soliton step length, we propose tuning the pump and auxiliary lasers synchronously. The thermal effects caused by the auxiliary laser light dominate ω_0 , the frequency of the resonance, so ω_0 is actually controllable. Therefore, ω_p and ω_0 can be changed in a large range as long as the detuning $\delta = \omega_0 - \omega_p$ is maintained. This method can greatly extend the absolute range of soliton existence. The operations are very easy based on our computer-controlled system.

First, we measure the soliton step length when the auxiliary laser stays still. After obtaining the single soliton, we can move the pump frequency on the soliton step. When the pump moves too far towards the low-frequency (red) direction and makes the detuning greater than the maximum which is determined by the pump power, the soliton vanishes. When the pump moves towards the high-frequency (blue) direction, we get breathing soliton [4]. In our experiments, transition from stable single soliton state to breathing soliton state is deterministic via tuning the pump laser towards blue direction. It agrees with the stability analysis of Lugiato-Lefever equation [40,41]. The breathing soliton can be easily distinguished from the stable soliton for its triangular spectrum [42] shown in Fig. 4(e). The beat note of one comb line of breathing soliton and a CW laser, which is shown in Fig. 4(f), indicates 500 MHz fundamental breathing frequency [42]. What is more, the intracavity power fluctuation can be detected by the power meter. Though the power meter (1 kSa/s) can only record irregular power fluctuation, The standard deviation of output power is apparently high in the breathing soliton state, as shown in Fig. 4(a). If the pump frequency moves further, it returns to the blue detuning area and destroys the soliton state. Therefore, we define the soliton step length as the range from the boundary of breathing and stable soliton to the soliton annihilation for excessive detuning.

We utilize the characteristics of the breathing soliton to measure the soliton step length. In the cases that the soliton disappears, and that the pump frequency enters the blue detuning area, the soliton cannot be restored by tuning the pump back. However, the stable single soliton state can be restored directly from the breathing soliton state by increasing the detuning. Therefore, to measure the maximum range of soliton step in one sweep, we first move the pump frequency towards the blue direction to transform the stable single soliton into the breathing soliton, and then move the pump towards the red direction until the soliton disappears, as shown in Fig. 4(a). In this way, both borders of the soliton step can be recorded in one single sweep. Under our experiment conditions (the on-chip pump power is 26 dBm), the soliton step length is ~ 700 MHz (frequency scan from 200 MHz to 900 MHz in Fig. 4(a)).

Then, we try to tune the auxiliary laser synchronously to expand the soliton step length. Whether the stable soliton state can be maintained is determined by the detuning $\delta = \omega_0 - \omega_p$, where the resonant frequency ω_0 is largely affected by the thermal effect of auxiliary laser. Hence, we believe that as long as the pump and auxiliary lasers are tuned synchronously to maintain a certain detuning, it will be possible to scan the pump frequency in a wide range. Theoretically, the moving speed of ω_0 is not the same as the tuning speed of the auxiliary laser. But experiments prove that tuning the two lasers with the same speed achieves a result good enough. The soliton step length exceeds 10 GHz (frequency scan from 0 MHz to 10500 MHz), as shown in Fig. 4(b).

In addition, we measure background noise power P_{noise} . Unlike the situation where we make the auxiliary laser stay still to measure soliton step length, here P_{noise} changes along with auxiliary laser frequency, because light generated by nonlinear effects of the auxiliary laser is reflected and

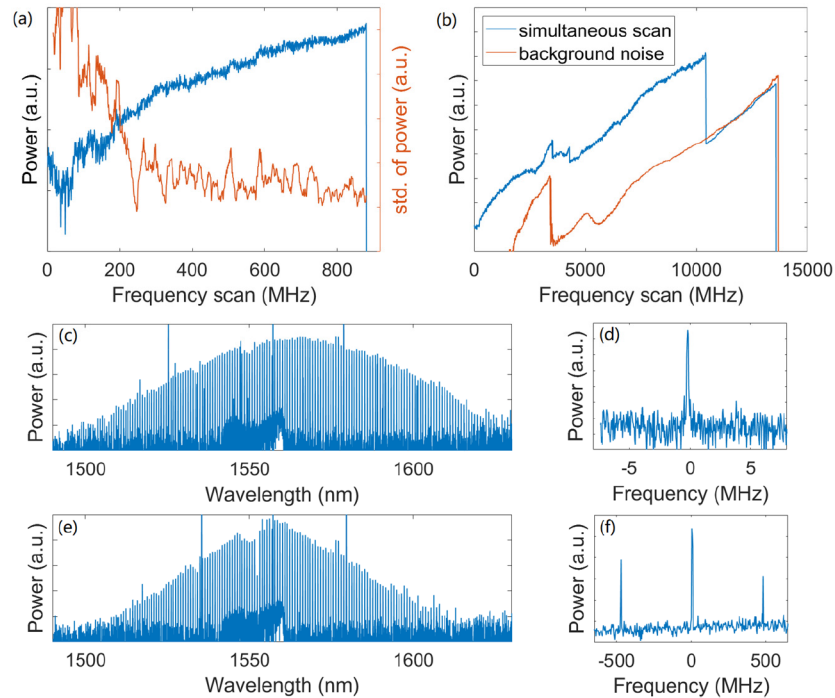


Fig. 4. (a) Output power of the system (blue) and the standard deviation of neighboring 15 samples of output power (red) in 0.05 mW/div. Only the pump laser is tuned while the auxiliary laser stays still. (b) Output power of the system in 0.05 mW/div. The blue curve shows that the pump and auxiliary laser are tuned synchronously. The red curve shows that only the auxiliary laser is tuned when the pump laser stays still, representing background noise power. (c) The spectrum of stable soliton state in 5 dB/div. (d) The beat note of one comb line of stable soliton and a CW laser in 5 dB/div. Central frequency of the beat note is 10.22 GHz. RBW = 100 kHz. (e) The spectrum of breathing soliton state in 5 dB/div. (f) The beat note of one comb line of breathing soliton and a CW laser in 5 dB/div. Central frequency of the beat note is 9.82 GHz. RBW = 100 kHz.

scattered to the soliton output port, thus detected by the power meter. The trend of P_{noise} is shown in Fig. 4(b). It increases as the auxiliary laser gets closer to the resonance, indicating that stronger and stronger nonlinear effects are excited. Then it drops suddenly, as shown in Fig. 4(b) the red line at 13500 MHz, indicating that the auxiliary laser reaches the red detuning area and loses its thermal effect. The theoretical limit of the excursion bandwidth that our scheme can achieve is from the frequency at which the auxiliary laser exiting the resonance, to the frequency at which the auxiliary laser gets over the resonance. However, the single soliton state may be destroyed by the cross-modulation between the auxiliary laser light and the soliton before reaching the limit, as shown in Fig. 4(b).

4. Conclusion

In conclusion, we develop a computer-controlled dual-laser DKS comb system for robust and automatic soliton generation. Two lasers and a power meter are controlled by the computer in this system. The system first automatically finds the frequency of a resonance by differentiating the transmission waveforms of the auxiliary laser scan. Then it infers whether the pump laser reaches the single soliton state by two criteria: the absolute power reading and the ratio of power

drop. The system can also rerun the automation script after the soliton vanishes. A few GHz frequency drift of the resonance, or $\pm 20\%$ pump power drift can be tolerated. It shows that our system has high robustness. The integrated modules including two lasers and a power meter used in the system reduce costs and miniaturize the system, which benefit to its production and application in industry. Furthermore, we use this computer-controlled system to tune two lasers synchronously in order to expand the excursion bandwidth. We easily expand the excursion bandwidth from 700 MHz to over 10 GHz. The method can be applied in many fields where wide excursion bandwidth is needed. What is more, for the system can flexibly control the frequency and output power of the lasers, it allows arbitrary and programmable switching of states on the soliton stability chart [41].

As our computer-controlled system is low-cost, integrated, and requires little manual operations, it can be applied in industrial fields like FMCW LiDAR. The system is packaged to the extent that non-professionals can operate it. Besides, it is possible to further automate and integrate our system. Electrically controlled FPCs can be used to make our system fully automatic. It can completely eliminate manual operations in our system and speed up soliton generation. The programs implemented on MCU instead of on a PC will help further integration.

Funding. Key-Area Research and Development Program of Guangdong Province (2018B030325002); National Natural Science Foundation of China (62075129).

Acknowledgments. The authors thank Prof. Heng Zhou and his team of UESTC for discussions on the optical frequency comb experiment schemes.

Disclosures. The authors declare no conflicts of interest.

Data availability. The code used to automate soliton generation in this paper are available in [Code 1](#), Ref. [37]. Data used in this study are available from the corresponding authors upon reasonable request.

References

1. S. T. Cundiff and J. Ye, "Colloquium: Femtosecond optical frequency combs," *Rev. Mod. Phys.* **75**(1), 325–342 (2003).
2. R. Holzwarth, Th. Udem, T. W. Hänsch, J. C. Knight, W. J. Wadsworth, and P. St. J. Russell, "Optical frequency synthesizer for precision spectroscopy," *Phys. Rev. Lett.* **85**(11), 2264–2267 (2000).
3. T. Herr, V. Brasch, J. D. Jost, C. Y. Wang, N. M. Kondratiev, M. L. Gorodetsky, and T. J. Kippenberg, "Temporal solitons in optical microresonators," *Nat. Photonics* **8**(2), 145–152 (2014).
4. T. J. Kippenberg, A. L. Gaeta, M. Lipson, and M. L. Gorodetsky, "Dissipative Kerr solitons in optical microresonators," *Science* **361**(6402), eaan8083 (2018).
5. P. Marin-Palomo, J. N. Kemal, M. Karpov, A. Kordts, J. Pfeifle, M. H. P. Pfeiffer, P. Trocha, S. Wolf, V. Brasch, M. H. Anderson, R. Rosenberger, K. Vijayan, W. Freude, T. J. Kippenberg, and C. Koos, "Microresonator-based solitons for massively parallel coherent optical communications," *Nature* **546**(7657), 274–279 (2017).
6. P. Trocha, M. Karpov, D. Ganin, M. H. P. Pfeiffer, A. Kordts, S. Wolf, J. Krockenberger, P. Marin-Palomo, C. Weimann, S. Randel, W. Freude, T. J. Kippenberg, and C. Koos, "Ultrafast optical ranging using microresonator soliton frequency combs," *Science* **359**(6378), 887–891 (2018).
7. M.-G. Suh and K. J. Vahala, "Soliton microcomb range measurement," *Science* **359**(6378), 884–887 (2018).
8. J. Riemensberger, A. Lukashchuk, M. Karpov, W. Weng, E. Lucas, J. Liu, and T. J. Kippenberg, "Massively parallel coherent laser ranging using a soliton microcomb," *Nature* **581**(7807), 164–170 (2020).
9. W. Liang, D. Eliyahu, V. S. Ilchenko, A. A. Savchenkov, A. B. Matsko, D. Seidel, and L. Maleki, "High spectral purity Kerr frequency comb radio frequency photonic oscillator," *Nat. Commun.* **6**(1), 7957 (2015).
10. D. T. Spencer, T. Drake, T. C. Briles, J. Stone, L. C. Sinclair, C. Fredrick, Q. Li, D. Westly, B. R. Ilic, A. Bluestone, N. Volet, T. Komljenovic, L. Chang, S. H. Lee, D. Y. Oh, M.-G. Suh, K. Y. Yang, M. H. P. Pfeiffer, T. J. Kippenberg, E. Norberg, L. Theogarajan, K. Vahala, N. R. Newbury, K. Srinivasan, J. E. Bowers, S. A. Diddams, and S. B. Papp, "An optical-frequency synthesizer using integrated photonics," *Nature* **557**(7703), 81–85 (2018).
11. M.-G. Suh, Q.-F. Yang, K. Y. Yang, X. Yi, and K. J. Vahala, "Microresonator soliton dual-comb spectroscopy," *Science* **354**(6312), 600–603 (2016).
12. M. Yu, Y. Okawachi, A. G. Griffith, N. Picqué, M. Lipson, and A. L. Gaeta, "Silicon-chip-based mid-infrared dual-comb spectroscopy," *Nat. Commun.* **9**(1), 1869 (2018).
13. F.-X. Wang, W. Wang, R. Niu, X. Wang, C.-L. Zou, C.-H. Dong, B. E. Little, S. T. Chu, H. Liu, P. Hao, S. Liu, S. Wang, Z.-Q. Yin, D.-Y. He, W. Zhang, W. Zhao, Z.-F. Han, G.-C. Guo, and W. Chen, "Quantum key distribution with on-chip dissipative Kerr soliton," *Laser Photonics Rev.* **14**(2), 1900190 (2020).
14. Y. He, Q.-F. Yang, J. Ling, R. Luo, H. Liang, M. Li, B. Shen, H. Wang, K. Vahala, and Q. Lin, "Self-starting bi-chromatic LiNbO₃ soliton microcomb," *Optica* **6**(9), 1138–1144 (2019).

15. X. Yi, Q.-F. Yang, K. Y. Yang, M.-G. Suh, and K. Vahala, "Soliton frequency comb at microwave rates in a high-Q silica microresonator," *Optica* **2**(12), 1078–1085 (2015).
16. V. Brasch, M. Geiselmann, T. Herr, G. Lihachev, M. H. P. Pfeiffer, M. L. Gorodetsky, and T. J. Kippenberg, "Photonic chip-based optical frequency comb using soliton cherenkov radiation," *Science* **351**(6271), 357–360 (2016).
17. L. Chang, W. Xie, H. Shu, Q.-F. Yang, B. Shen, A. Boes, J. D. Peters, W. Jin, C. Xiang, S. Liu, G. Moille, S.-P. Yu, X. Wang, K. Srinivasan, S. B. Papp, K. Vahala, and J. E. Bowers, "Ultra-efficient frequency comb generation in AlGaAs-on-insulator microresonators," *Nat. Commun.* **11**(1), 1331 (2020).
18. Z. Gong, A. Bruch, M. Shen, X. Guo, H. Jung, L. Fan, X. Liu, L. Zhang, J. Wang, J. Li, J. Yan, and H. X. Tang, "High-fidelity cavity soliton generation in crystalline AlN micro-ring resonators," *Opt. Lett.* **43**(18), 4366–4369 (2018).
19. V. Brasch, M. Geiselmann, M. H. P. Pfeiffer, and T. J. Kippenberg, "Bringing short-lived dissipative Kerr soliton states in microresonators into a steady state," *Opt. Express* **24**(25), 29312–29320 (2016).
20. H. Guo, M. Karpov, E. Lucas, A. Kordts, M. H. P. Pfeiffer, V. Brasch, G. Lihachev, V. E. Lobanov, M. L. Gorodetsky, and T. J. Kippenberg, "Universal dynamics and deterministic switching of dissipative Kerr solitons in optical microresonators," *Nat. Phys.* **13**(1), 94–102 (2017).
21. E. Obrzud, S. Lecomte, and T. Herr, "Temporal solitons in microresonators driven by optical pulses," *Nat. Photonics* **11**(9), 600–607 (2017).
22. Y. Bai, M. Zhang, Q. Shi, S. Ding, Y. Qin, Z. Xie, X. Jiang, and M. Xiao, "Brillouin-Kerr soliton frequency combs in an optical microresonator," *Phys. Rev. Lett.* **126**(6), 063901 (2021).
23. T. Wildi, V. Brasch, J. Liu, T. J. Kippenberg, and T. Herr, "Thermally stable access to microresonator solitons via slow pump modulation," *Opt. Lett.* **44**(18), 4447–4450 (2019).
24. C. Joshi, J. K. Jang, K. Luke, X. Ji, S. A. Miller, A. Klenner, Y. Okawachi, M. Lipson, and A. L. Gaeta, "Thermally controlled comb generation and soliton modelocking in microresonators," *Opt. Lett.* **41**(11), 2565–2568 (2016).
25. S. Zhang, J. M. Silver, L. D. Bino, F. Copie, M. T. M. Woodley, G. N. Ghalanos, A. Ø. Svela, N. Moroney, and P. Del'Haye, "Sub-milliwatt-level microresonator solitons with extended access range using an auxiliary laser," *Optica* **6**(2), 206–212 (2019).
26. H. Weng, J. Liu, A. A. Afridi, J. Li, J. Dai, X. Ma, Y. Zhang, Q. Lu, J. F. Donegan, and W. Guo, "Directly accessing octave-spanning dissipative Kerr soliton frequency combs in an AlN microresonator," *Photonics Res.* **9**(7), 1351–1357 (2021).
27. H. Zhou, Y. Geng, W. Cui, S.-W. Huang, Q. Zhou, K. Qiu, and C. W. Wong, "Soliton bursts and deterministic dissipative Kerr soliton generation in auxiliary-assisted microcavities," *Light: Sci. Appl.* **8**(1), 50 (2019).
28. Y. Geng, W. Cui, J. Sun, X. Chen, X. Yin, G. Deng, Q. Zhou, and H. Zhou, "Enhancing the long-term stability of dissipative Kerr soliton microcomb," *Opt. Lett.* **45**(18), 5073–5076 (2020).
29. Z. Lu, H.-J. Chen, W. Wang, L. Yao, Y. Wang, Y. Yu, B. E. Little, S. T. Chu, Q. Gong, W. Zhao, X. Yi, Y.-F. Xiao, and W. Zhang, "Synthesized soliton crystals," *Nat. Commun.* **12**(1), 3179 (2021).
30. Y. Zhao, L. Chen, C. Zhang, W. Wang, H. Hu, R. Wang, X. Wang, S. T. Chu, B. Little, W. Zhang, and X. Zhang, "Soliton burst and bi-directional switching in the platform with positive thermal-refractive coefficient using an auxiliary laser," *Laser Photonics Rev.* **15**(11), 2100264 (2021).
31. S. Zhang, J. M. Silver, T. Bi, and P. Del'Haye, "Spectral extension and synchronization of microcombs in a single microresonator," *Nat. Commun.* **11**(1), 6384 (2020).
32. X. Wang, P. Xie, W. Wang, Y. Wang, Z. Lu, L. Wang, S. T. Chu, B. E. Little, W. Zhao, and W. Zhang, "Program-controlled single soliton microcomb source," *Photonics Res.* **9**(1), 66–72 (2021).
33. N. Kuse, T. C. Briles, S. B. Papp, and M. E. Fermann, "Control of Kerr-microresonator optical frequency comb by a dual-parallel Mach-Zehnder interferometer," *Opt. Express* **27**(4), 3873–3883 (2019).
34. K. Nishimoto, K. Minoshima, T. Yasui, and N. Kuse, "Generation of a microresonator soliton comb via current modulation of a DFB laser," *OSA Continuum* **3**(11), 3218–3224 (2020).
35. R. Niu, S. Wan, J. Li, R.-C. Zhao, C.-L. Zou, G.-C. Guo, and C.-H. Dong, "Fast Spectroscopy Based on a Modulated Soliton Microcomb," *IEEE Photonics J.* **13**, 1–4 (2021).
36. N. Kuse, G. Navickaite, M. Geiselmann, T. Yasui, and K. Minoshima, "Frequency-scanned microresonator soliton comb with tracking of the frequency of all comb modes," *Opt. Lett.* **46**(14), 3400–3403 (2021).
37. L. Zhou, "Computer-controlled microresonator soliton comb system automating soliton generation," GitHub (2022), <https://github.com/QNPsjtu/AutoSoliton>.
38. J. R. Stone, T. C. Briles, T. E. Drake, D. T. Spencer, D. R. Carlson, S. A. Diddams, and S. B. Papp, "Thermal and nonlinear dissipative-soliton dynamics in Kerr-microresonator frequency combs," *Phys. Rev. Lett.* **121**(6), 063902 (2018).
39. M. Karpov, H. Guo, A. Kordts, V. Brasch, M. H. P. Pfeiffer, M. Zervas, M. Geiselmann, and T. J. Kippenberg, "Raman self-frequency shift of dissipative Kerr solitons in an optical microresonator," *Phys. Rev. Lett.* **116**(10), 103902 (2016).
40. F. Leo, L. Gelens, P. Emplit, M. Haelterman, and S. Coen, "Dynamics of one-dimensional Kerr cavity solitons," *Opt. Express* **21**(7), 9180–9191 (2013).
41. C. Godey, I. V. Balakireva, A. Coillet, and Y. K. Chembo, "Stability analysis of the spatiotemporal Lugiato-Lefever model for Kerr optical frequency combs in the anomalous and normal dispersion regimes," *Phys. Rev. A* **89**(6), 063814 (2014).
42. E. Lucas, M. Karpov, H. Guo, M. L. Gorodetsky, and T. J. Kippenberg, "Breathing dissipative solitons in optical microresonators," *Nat. Commun.* **8**(1), 736 (2017).